ORIGINAL ARTICLE

Double-sided hybrid laser-MIG welding plus MIG welding of 30-mm-thick aluminium alloy

Zhao Jiang[1,2] · Xueming Hua[1,2] · Lijin Huang[1,2] · Dongsheng Wu[1,2] · Fang Li[1,2] · Yuelong Zhang[1,2]

Abstract

Hybrid laser-MIG (metal inert gas) welding has not been extensively applied in welding of aluminium alloy with thickness more than 10 mm because of the existence of weld defects and low joint strength. In this study, an original hybrid laser-MIG welding plus MIG welding process was developed. Double-sided hybrid laser-MIG welding method was designed and applied to the welding of 30-mm-thick Al 5083 alloy. The process was then optimized by overlaying a MIG welding upon the weld. Analysis on the weld revealed that the overlaid MIG welding played multiple roles, including making up the bead formations, eliminating the keyhole-induced porosities as well as refining grains. Along the longitudinal direction of the weld, the grains became finer from two fringes to the middle, and the mechanical properties improved accordingly. Compared with MIG welding, the hybrid laser-MIG welding plus MIG welding process showed overwhelming superiorities over the MIG welding, which will be promising in industrial applications.

Keywords Hybrid laser-MIG welding plus MIG welding · Double-sided welding · Porosity · Al 5083 alloy

1 Introduction

Thick Al 5083 alloy plates have been widely applied in liquefied natural gas transports and storage tanks owing to its low specific weight, excellent low-temperature toughness and corrosion resistance in marine environments. At present, metal inert gas (MIG) welding is the most commonly used process during the joining of thick Al 5083 alloy plates. However, the trivial bevel preparation [1, 2], complicated multi-pass process [3] and high heat input accompanied with large distortion greatly restrict the welding efficiency and weld quality.

In order to improve the welding efficiency and bead formation, hybrid laser-MIG welding has been introduced to thick plate welding. The high power density of the laser beam can achieve great penetration easily, simplifying the welding process and improving the production efficiency remarkably.

Meanwhile, the arc working upon the weld surface contributes to sound bead appearance. Many researches have been done to investigate the coupling effect between laser and arc [4], the weld pool characteristic [5], the microstructure [6] as well as the mechanical strength [7] during hybrid laser-MIG welding of aluminium alloy. Nevertheless, some challenges have not been satisfactorily solved yet. Among which, keyhole-induced porosity originating from the frequent collapses of the keyhole is a serious problem leading to the deterioration of mechanical properties. The mechanism of porosity formation suggests that the weld metal solidifies more rapidly than the possible rise velocity of the gas bubbles that formed during keyhole collapse, resulting in severe porosity [8]. In order to work out this problem, a series of factors were investigated such as laser parameters [9], welding speed [10], shielding gas [11], distance between laser and arc [11] and power distribution [12]. It seemed difficult to completely avoid the porosity during hybrid laser-MIG welding process of aluminium alloy.

Another serious issue is the bead formation. During hybrid laser-MIG welding of aluminium alloy, the drastic and unstable melt flow and the complicated interaction between heat source and melt pool make the undercut and the underfill occur easily. Besides, high-energy density laser beam usually gives rise to strong spatter [13], resulting in bad bead formation. Root sagging is easily produced in full-penetration joint

✉ Xueming Hua
xmhua@sjtu.edu.cn

1 Shanghai Key Laboratory of Materials Laser Processing and Modification, Shanghai Jiao Tong University, Shanghai 200240, People's Republic of China

2 Collaborative Innovation Centre for Advanced Ship and Deep-Sea Exploration, Shanghai 200240, People's Republic of China

on account of the high penetration capability of laser beam and the good fluidity of aluminium alloy. The formation of root sagging is attributed to the imbalance between the gravity of liquid metal in the weld pool and the surface tension [14]. Despite being able to avoid the root sagging with the support of the backing strap or the external electromagnetic field [15], they increase the complexity and production costs obviously.

Restricting by the formed weld defects mentioned above and the available laser power, the majority of current investigations on hybrid laser-MIG welding of aluminium alloy focus on thin plate with thickness no more than 10 mm [11, 16], which neither allows full play to the advantage of hybrid laser-MIG welding nor meets the needs of large-scale engineering application. In this study, an original "hybrid laser-MIG welding plus MIG welding" process was developed. The 30-mm-thick Al 5083 alloy plates are jointed by double-sided hybrid laser-MIG welding method. Then, welding defects are worked out and the welding parameters are optimized on the basis of analysis concerning the mechanism of defect formation and its distribution. Afterwards, the distribution of microstructure and mechanical properties along the longitudinal direction of weld is studied to characterize the heterogeneity of the weld. A comprehensive comparison between MIG welding and hybrid laser-MIG welding plus MIG welding is made to better manifest the advantages of the latter.

2 Materials and methods

The base material used was Al 5083 alloy with thickness 20 mm (bead-on-plate welding) and 30 mm (butt welding). The filler used was ER5183 wire with diameter 1.2 mm during hybrid laser-MIG welding and 1.6 mm during MIG welding. The chemical compositions of Al 5083 alloy and ER5183 wire are given in Table 1. The shielding gas used was pure argon with flow rate 15.0 L/min. Hybrid laser-MIG welding was conducted using a 10 kW continuous wave IPG Photonics Yb-fiber laser and Fronius TransPuls Synergic 5000 CMT welding power source. The laser beam energy in the focused spot presented Gauss-like distribution. Some parameters about the laser beam were

listed as follows: wavelength, 1070 nm; focal radius, 0.36 mm; and beam parameter product, 12.5 mm × mrad. Some welding parameters that remained constant during the whole welding process are presented schematically in Fig. 1.

The main route of the research was as follows. To begin with, considering the limited laser power (10 kW) yet the thick butt joint (30 mm), the work concentrated on accomplishing the maximum weld penetration. Afterwards, the double-sided welding method was designed and employed to the butt welding of Al 5083 alloy with thickness 30 mm. For the sake of subsequent optimization, porosity was controlled to appear only on surface locations of the weld by regulation of process parameters. The influences of groove type on porosity and bead formation were discussed. Following which, the MIG welding was overlaid on the original weld so as to improve the bead formation and wipe out the porosity completely, which yielded the perfect weld finally. Then an exhaustive analysis about the weld was conducted.

Specimens for macroscopic and microscopic investigations were prepared according to standard metallographical techniques. Macroscopic cross sections were etched by hydrofluoric acid solution (10%) and observed by optical microscope of Zeiss Stemi2000. Metallographic specimens were prepared by anodic oxidation method with the electrolyte of boratofluoric acid (2.5%) for about 90 s. Observation of microstructure was carried out by polarizing microscope (Leica DM4000) under orthogonal polarizing system. Microhardness was measured by automatic Vickers hardness tester (Zwick/Roell ZHμ, HVμ-A) with the load 500 g and dwell time 15 s. Tensile specimens were prepared in accordance with ISO 6982-1:2009 standards. The tensile machine of Zwick/Roell Z100 was applied to the measurement of mechanical properties with the strain rate 2.0 mm/min.
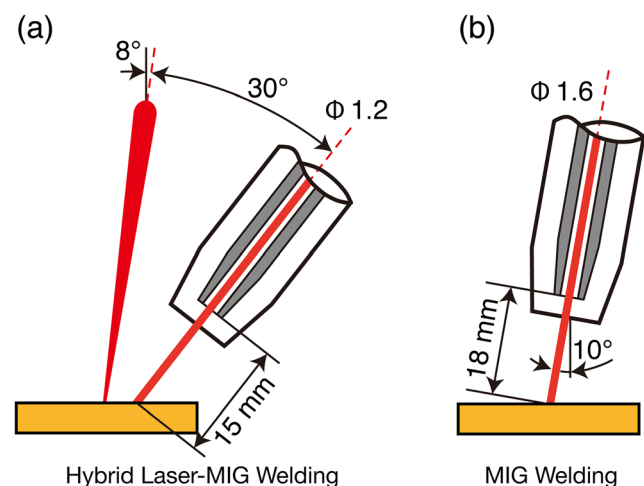
Table 1 Chemical compositions of base metal 5083 and filler ER5183 (wt%)

Elements	Mg	Mn	Si	Fe	Ti	Zn	Cu	Cr	Al
Base metal	4.50	0.70	0.40	0.40	0.25	0.25	0.15	0.25	Bal.
Filler metal	4.80	0.70	0.09	0.20	0.15	0.10	0.08	0.15	Bal.

Fig. 1 Welding parameters remaining unchanged during **a** hybrid laser-MIG welding and **b** MIG welding

3 Results and discussion

3.1 Obtaining the maximum weld penetration

This study aimed at the high-quality and efficient butt welding of 30-mm-thick plate; unfortunately, the 30-mm-thick plate could never be penetrated on account of the limited laser power. Therefore, prior to butt welding of the thick plate, the bead-on-plate welding was conducted to obtain the maximum weld penetration under present circumstance. Figure 2 shows the weld profiles with various leading modes, defocusing distance (D_F) and the distance between laser and arc (D_{LA}), with remaining laser power (10 kW), welding current (150 A), welding speed (1.5 m/min), as well as wire feeding rate (9.2 m/min) unchanged. As demonstrated, different leading modes showed almost no distinction in weld penetration, but the laser leading configuration produced a sounder weld with less porosity and no undercut. Excessive defocusing could reduce the weld penetration rapidly. By comparison, no defocusing or appropriate negative defocusing were beneficial to both weld penetration and bead appearance. With the increase of D_{LA}, the weld penetration reduced but the bead appearance improved gradually. The increased D_{LA} weakened the coupling effect between laser and arc, leading to the improvement of welding stability but the decrease of penetration. Considering both weld penetration and bead appearance, the laser leading configuration, the D_F 0 mm and the D_{LA} 2 mm were adopted for the experiments.

Three main parameters, i.e. laser power (P), welding speed (v) as well as welding current (I), were synthetically investigated by response surface methodology (RSM) to obtain the maximum weld penetration. Seeing that the RSM was well known and not the focus of this research, most details were left out. Figure 3 shows the weld cross sections acquired from the RSM design, from which it could be inferred the undercut and porosity were universal defects among hybrid laser-MIG welding weld. Attention should be paid to the porosity since they appeared merely on the upper sites of the weld. Based on the analysis to the established regression model, the optimal process parameter for maximum penetration was acquired, i.e. laser power 10 kW, welding speed 0.6 m/min and welding current 136 A. Figure 4 shows the weld cross section with maximum penetration 18 mm.

3.2 Double-sided hybrid laser-MIG welding of 30-mm-thick aluminium alloy

Based on above analysis, the weld penetration reached at 18 mm (larger than 15 mm) on condition of the designated parameters, signifying the thick section could be jointed by two welds. Hence, a double-sided welding method was put forward [17], that is, hybrid laser-MIG welding was performed on the top side, the plate was turned upside down next and the second hybrid laser-MIG welding pass was laid. Figure 5 schematically shows the double-sided hybrid laser-MIG welding process. An obvious advantage here was the root sagging defect needed not to take into consideration any more, since the laser beam did not fully penetrate the joint in the first pass. At the same time, no bevel was prepared and no

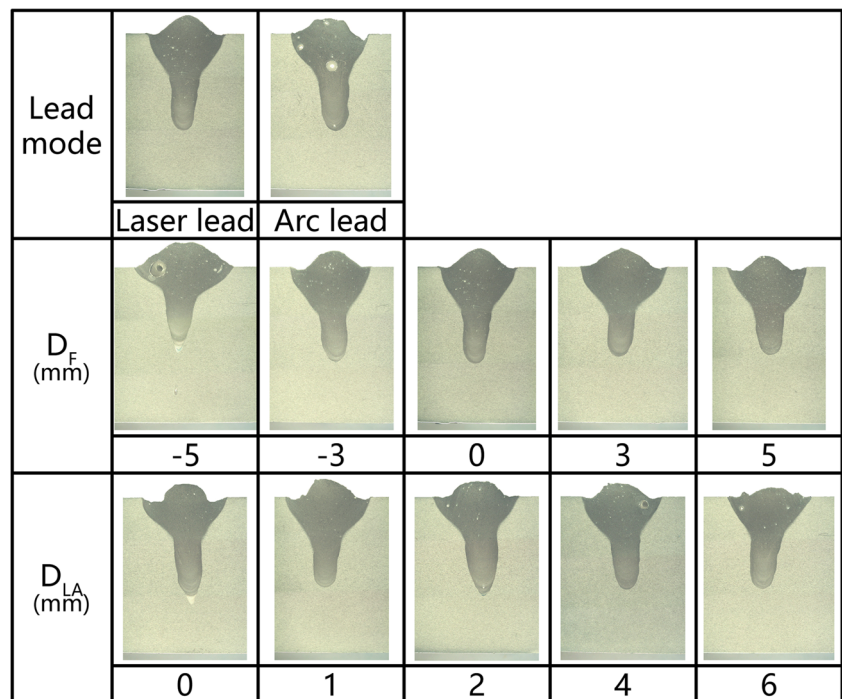**Fig. 2** Weld profiles with various leading mode, D_F and D_{LA}

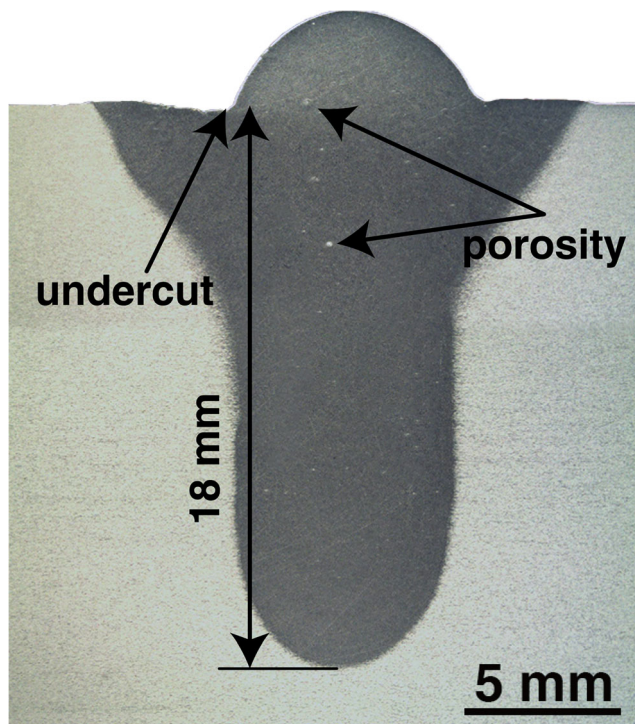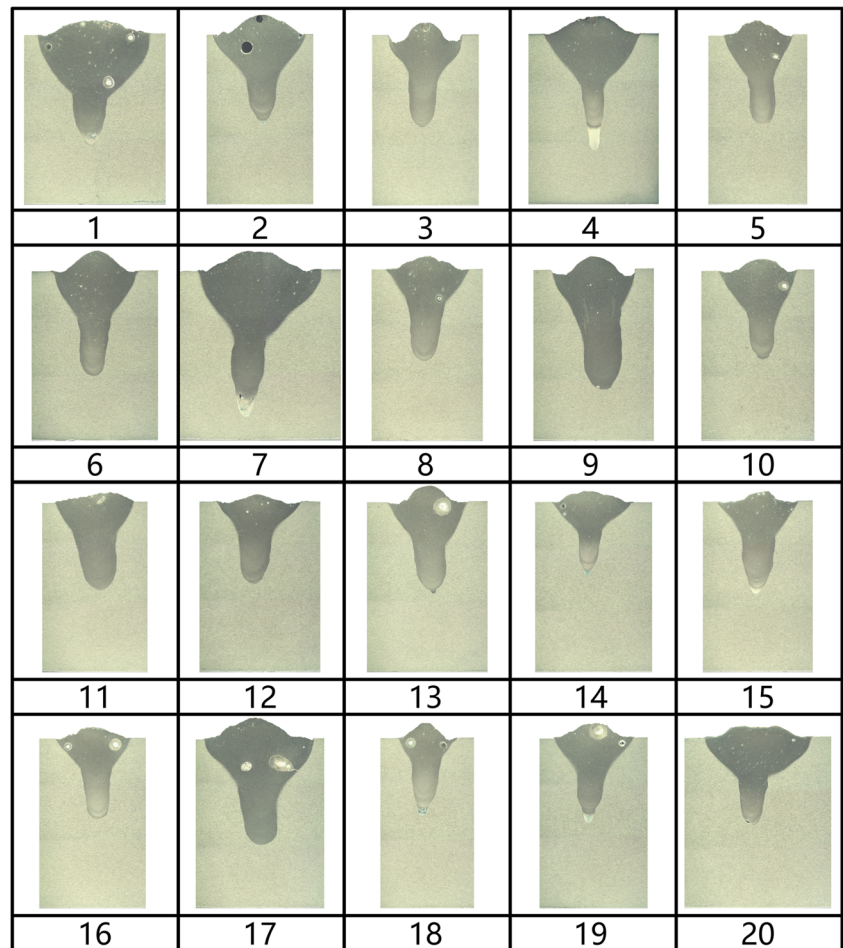**Fig. 3** Weld profiles for RSM design with 20 runs

gap was left for the groove on the consideration of simplicity and practicability.

Figure 6a shows the transverse section and longitudinal section of the weld from above process. The slight undercut was observed from the transverse section. A string of porosities appeared only on the top and bottom surfaces of the weld, meaning that the inside porosity was effectively wiped out as envisaged, which could facilitate subsequent complete elimination of these porosities. In order to improve the bead appearance and avoid the porosity, different groove types, including 60° bevel and 1.0 mm gap, were attempted, as shown in Fig. 6b–d, respectively. Clearly, the porosity was distributed on upper sites of the weld and showed no difference with respect to different groove types. However, the existence of gap or bevel exacerbated the weld undercut and even gave rise to the weld underfill. Since more metals were needed to fill the gap and the groove.

A unique phenomenon here was that all porosities appeared only on the surfaces of the weld, which was much different from forerunner's studies [11]. In the experiments, the welding speed selected was much less than that usually adopted by laser welding. Two key points caused by the low welding speed accounted for the special behaviour of porosity.

Fig. 4 The weld cross section with maximum penetration

Fig. 5 Double-sided hybrid laser-MIG welding process. **a** Top side. **b** Bottom side
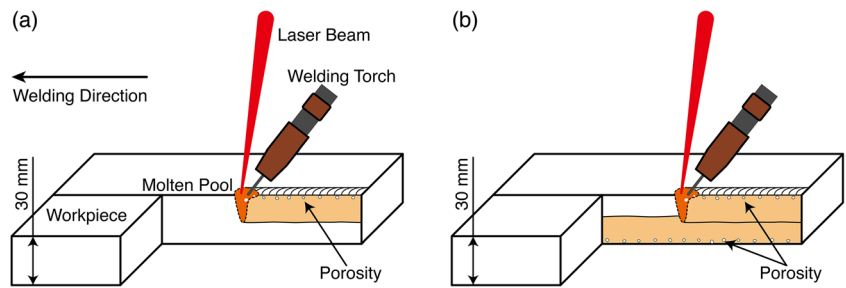
On the one hand, welding speed made a big difference to the weld pool profile. Faraji et al. [18] demonstrated that the weld pool half width decrease with increasing the welding speed, resulting in different weld profiles. For different welding speed scenarios, Fig. 7 presents the deference during the bubble escape from the molten pool. Obviously, the bubbles were very likely to be trapped in the weld with small half width. For the weld with large half width; however, bubbles could keep moving upward with the fluid, some of them got into the air and the other might be enveloped on the upper sites of the weld. What's more, according to the study of Zhang et al. [19], for the weld with large half width, the bubbles tended to have a short escaping distance and thus possessed higher possibility to escape away from molten pool to the air.

Fig. 6 Transverse section and longitudinal section of different groove types. **a** No gap, no bevel. **b** 0.7 mm gap, no bevel. **c** No gap, 60° bevel. **d** both 0.7 mm gap and 60° bevel
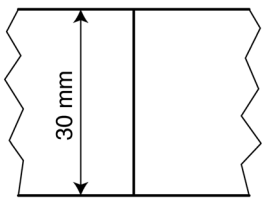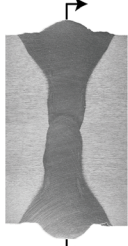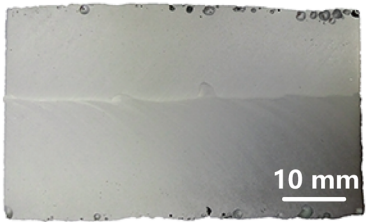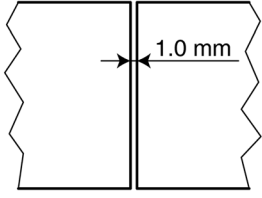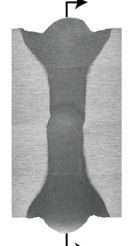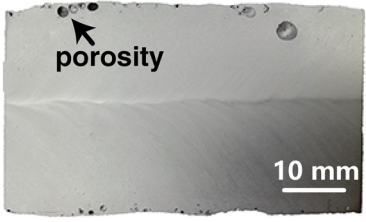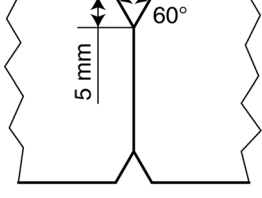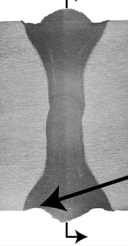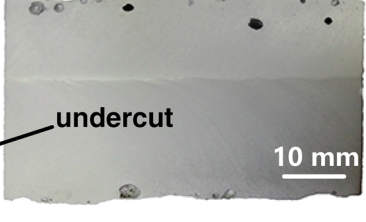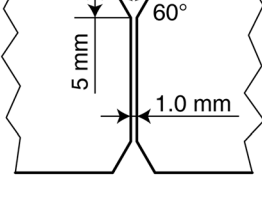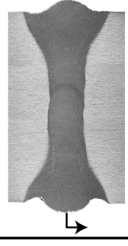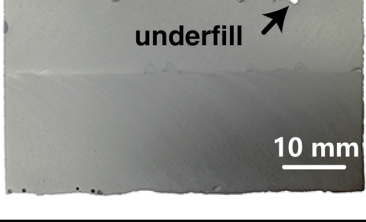
Fig. 7 Escape process of a bubble for different welding speed. **a** High welding speed. **b** Low welding speed
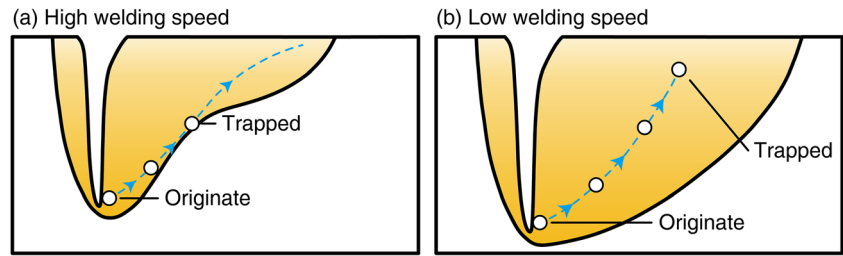
On the other hand, the adopted welding speed in the experiments was low indeed, which provided enough time for the bubbles to float up, even though some of them were trapped in the weld eventually. As a consequence, the porosities all distributed along the top and bottom sites of the weld.

3.3 Optimization of the double-sided hybrid laser-MIG welding process

Up to now, the plates could be jointed by the proposed double-sided welding method; the root sagging defect was avoided and the location of porosity was well controlled. Nevertheless, the defects of undercut, underfill and porosity still needed to be eliminated from the point of view of industrial application. It should be noted that both undercut and underfill belonged to surface defect. By coincidence, all porosities also existed only on the upper sites of the weld. It inspired a simple but practical idea that overlaying a weld on the top and bottom surfaces respectively by MIG welding. On the one hand, the added metal could make up the pits caused by undercut and underfill. On the other hand, those enveloped bubbles could be released and escape further under the re-melting action of arc on the surface weld metal. The welding process was denoted as hybrid laser-MIG welding plus MIG welding process. Figure 8a shows the escape process of enveloped bubbles after melted by arc, and Fig. 8b shows the overlaid MIG weld wiped out all porosities and contributed to perfect bead appearance without undercut and underfill.

Considering that some space was needed to accommodate the metal from subsequent MIG welding process and obtain appropriate weld reinforcement, two measures were taken, i.e. the groove type in Fig. 6c was adopted, and the current of hybrid laser-MIG welding process was optimized to 100 A. For the added MIG welding process, the welding current was 260 A, the amplitude of arc swing was 3.5 mm and the

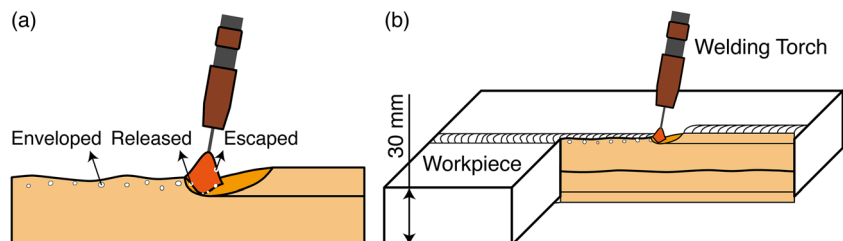welding torch travelled at a speed of 0.6 m/min. Figure 9a shows the groove type, the transverse section and the longitudinal section of the obtained perfect weld from the optimized process. No undercut, underfill and porosity were found from the sections. Figure 9b, c presents the bead appearance and the X-ray radiographic inspection result of the weld respectively. There was almost no porosity detected by X-ray radiographic. Only several were observed at the beginning and ending of the weld, resulted from the instabilities of arc striking and arc extinguishing.

3.4 Assessment of weld joint

This part aimed at the characterizations of the weld joint obtained from the optimized process. In order to figure out the effect of the overlaid MIG weld on the weld joint, the weld microstructures were compared between the plate welded by two hybrid welding processes and the plate welded by two hybrid welding processes as well as two MIG welding processes, as shown in Fig. 10a, b, respectively. In the laser zone, the difference of grain size was not distinct. In the arc zone, quite evidently, the grain size showed in Fig. 10a was larger than that showed in Fig. 10b. The heat source in MIG welding was not as strong as that in hybrid laser-MIG welding; besides, the welding torch had a swing amplitude of 3.5 mm in MIG welding process, so that the weld overlaid by MIG welding show a refined microstructure. Therefore, conclusion could be made that the overlaid MIG welding played multiple roles such as refining grains, eliminating the keyhole-induced porosities as well as improving the bead formations.

Figure 11 shows the microstructure that observed from seven representative positions of the weld cross section. For the arc zone, coarse columnar grains distributed along the fusion boundary (#3), and other areas were equiaxed grains (#2). Particularly, abnormal columnar grains constituted by many parallel strips were found in the middle part of the

Fig. 8 **a** Enveloped porosity was released and then escaped. **b** Wiping out porosity and improving bead appearance by overlaying a MIG weld

Fig. 9 **a** Transverse section and longitudinal section of the weld from optimized welding process. **b** Bead appearance. **c** X-ray radiographic inspection of the weld
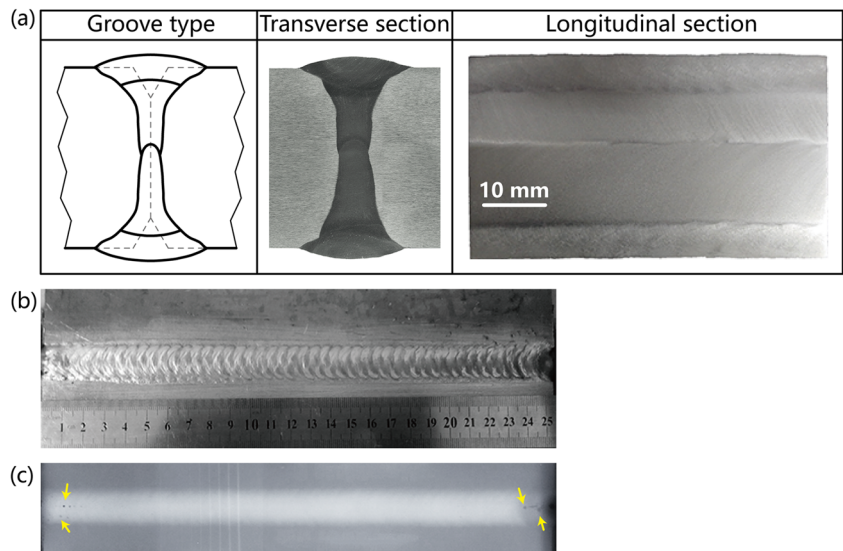

surface (#1), where solidification finally occurred. On the boundary between two welds (#4), the side closed to the arc zone was columnar grain, yet the other side closed to laser zone was equiaxed grain. Just below the boundary (#5), there existed a heat-affected zone (HAZ) caused by the heat source of arc, in which the coarse equiaxed grains were observed. As for the laser zone, the grain became finer and finer with approaching the weld tip (#6). The superfine grains were observed at the tip (#7) due to low heat input and fast cooling rate.

It was of great significance to figure out the specific differences of microstructure on account of the decisive role it played in mechanical properties of weld joint. Therefore, the grain size and its probability distribution of arc zone (Fig. 11, #2) and laser zone (Fig. 11, #7) were investigated. The grains of the former two zones were extracted randomly and then processed elaborately, as shown in Fig. 12a, c, correspondingly. Ultimately, the grain size was computed by Image-Pro Plus. Figure 12b, d shows the probability distribution of grain size in arc zone and laser zone, respectively. The average grain size of the laser zone, 26.25 μm, was approximately three times smaller than that of the arc zone, 69.80 μm, which might well predict the better performances of laser zone.

Fig. 10 Welds that welded by **a** two hybrid welding processes and **b** two hybrid welding processes as well as two MIG welding processes
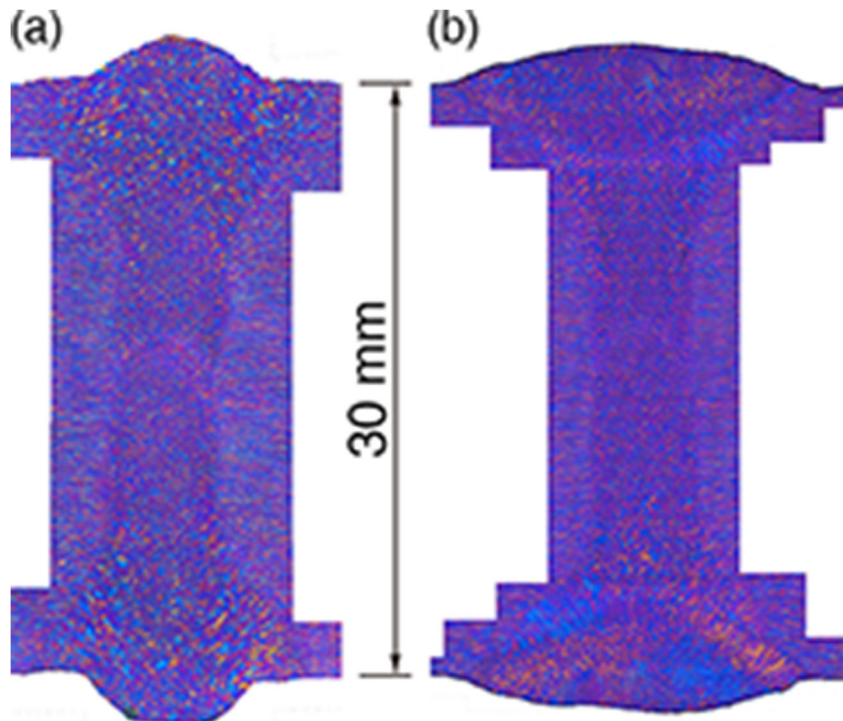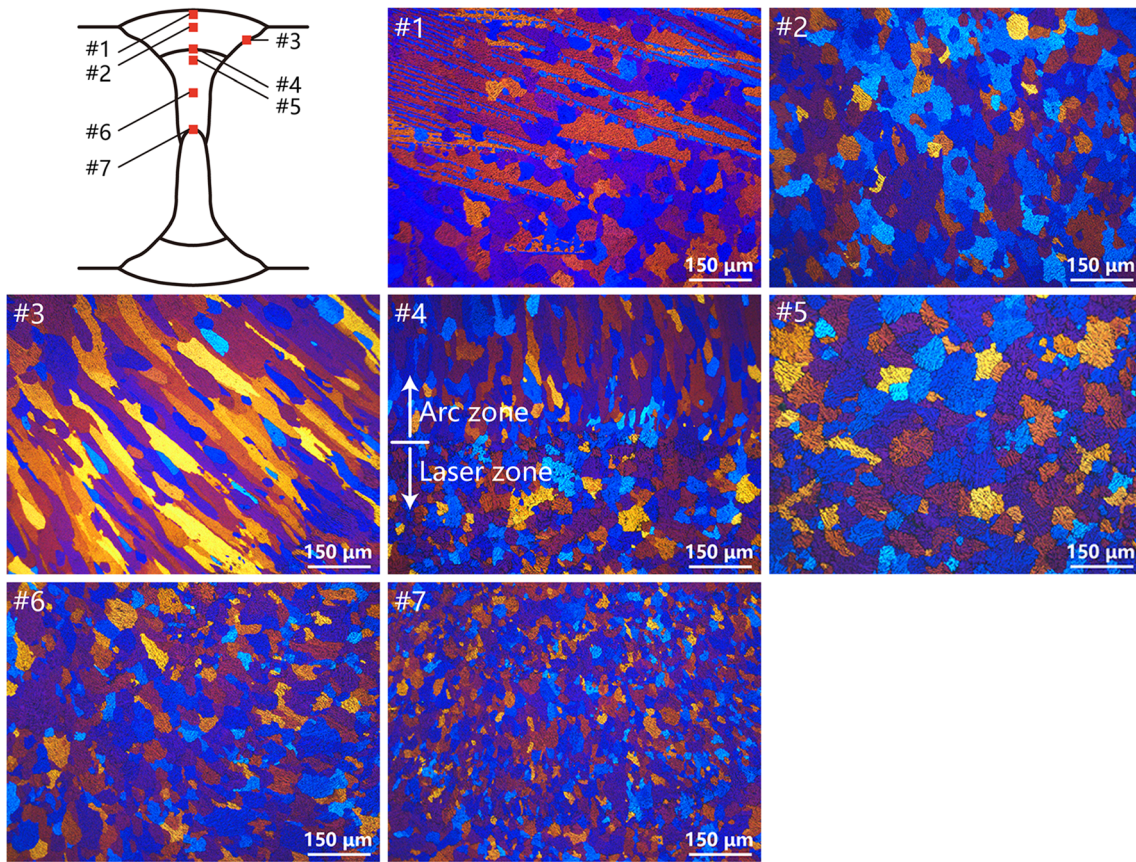
Fig. 11   Microstructure that observed from seven representative positions of the weld

Aforementioned discoveries about microstructure seemed to indicate the inhomogeneous performance of the weld joint. Therefore, microhardness was measured along the longitudinal direction of the weld. Figure 13 reveals the distribution of microhardness, in which these data points were fitted by quadratic curve. The red fitting curve demonstrated that, along the longitudinal direction, microhardness of the weld increased indeed from the two fringes to the middle. Apparently, the microhardness in laser zone was larger than that in arc zone. Just below the MIG weld, there existed a HAZ caused by the heat source of arc, whose microhardness was relatively low because of the coarsening of grains, as shown in Fig. 11, #5.

Fig. 12   a, c Extraction of grains; b, d Grain size and its probability distribution
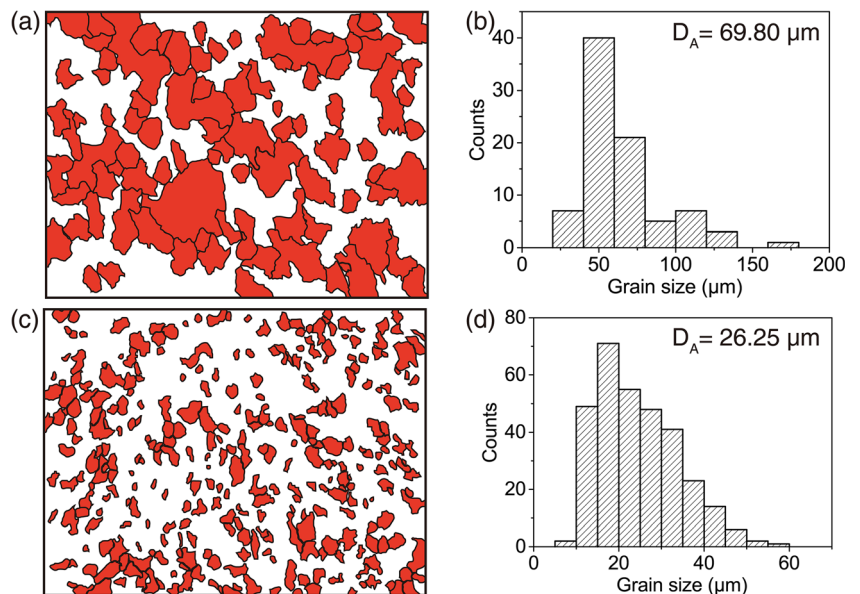
Fig. 13 **a** Test position of microhardness. **b** Microhardness distribution along the longitudinal direction of the weld

Consistently, tensile test was conducted at five different positions of the weld. Cartesian coordinate system was established along the longitudinal direction of the weld, as
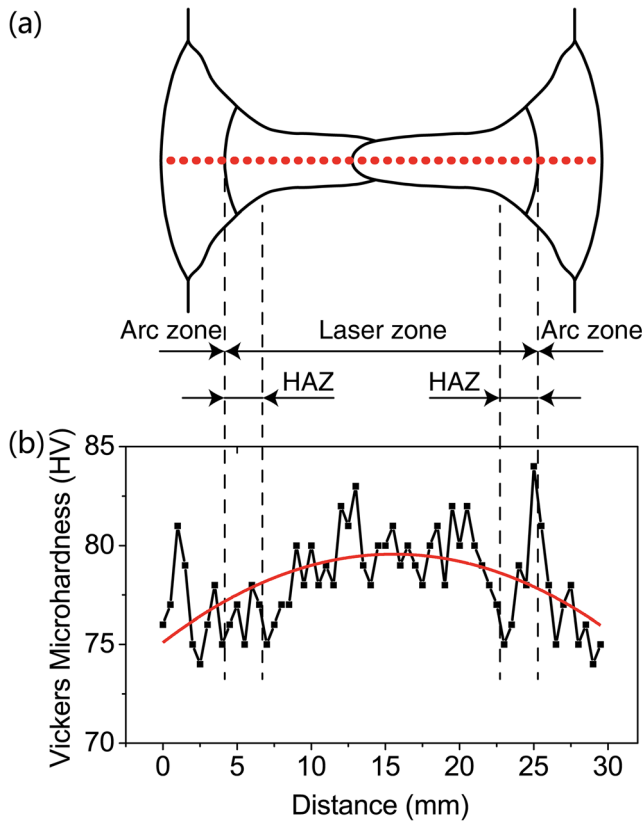
shown in Fig. 14a, in which the positions of five specimens and their serial numbers were marked out on the left and the right, respectively. All tested specimens failed in weld zone in the experiments, indicating the poorer performance of weld zone due to the softening effect [20, 21]. For three key mechanical parameters, i.e. elongation after fracture (A), 0.2% proof strength ($R_{P0.2}$) as well as the tensile strength (R_m), their scatter diagrams were plotted with the test positions, following with the parabola fitting of these data points. Figure 14b–d depicts the fitting curves and provided the fitting equations of the three mechanical parameters. The three parameters increased from two fringes to the middle of the weld, the same trend with microhardness showed in Fig. 13, which was attributed to the finer microstructure in the middle position of the weld.

3.5 Comparison between MIG welding and hybrid laser-MIG welding plus MIG welding

The author's previous work reported the MIG welding of 30-mm-thick Al 5083 alloy [22]. Now, a comparison between MIG welding and hybrid laser-MIG welding plus MIG welding could be made to see where the advantage of the latter was. Figure 15 shows the cross sections of the two kinds of weld, and Table 2 summarizes some items about the two welding processes. For convenience, the MIG welding process and the hybrid laser-MIG welding plus MIG welding process were represented by "M process" and "H process", respectively.

Fig. 14 **a** Sampling locations. **b–d** Parabola fitting of three mechanical parameters, A, $R_{P0.2}$ and R_m

$A = -0.009(X-2.22)^2 + 9.25$

$R_{P0.2} = -0.014(X+1.43)^2 + 202.49$
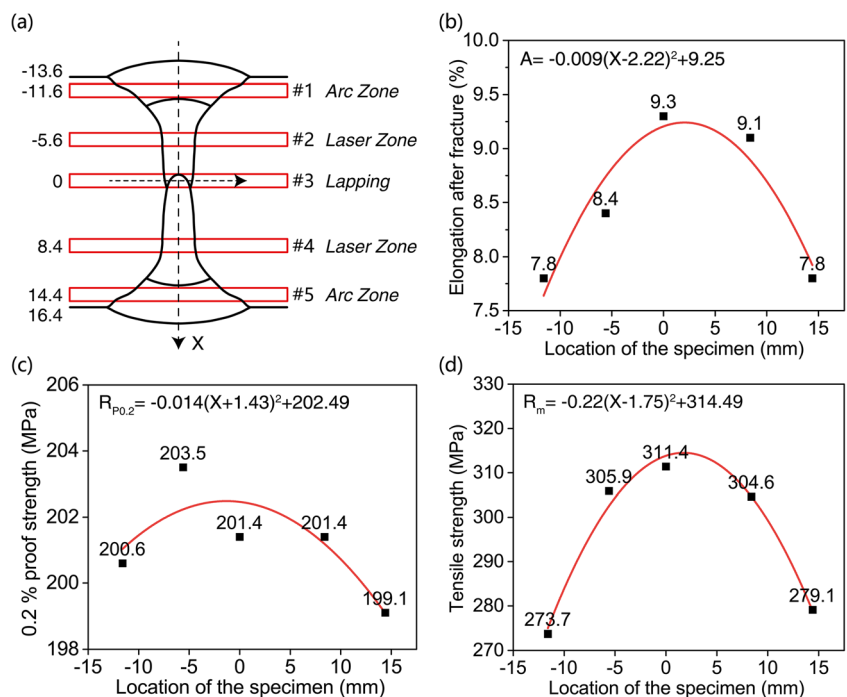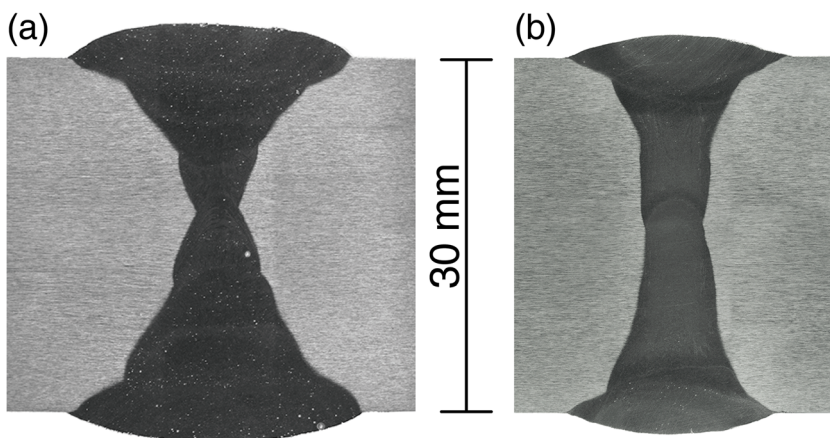
$R_m = -0.22(X-1.75)^2 + 314.49$

Fig. 15 Welds of **a** MIG welding and **b** hybrid laser-MIG welding plus MIG welding

For M process, a symmetric 60° V-type groove needed to be prepared; the groove area could be calculated as 227 mm^2. Large groove meant large amount of filler metal, more welding passes and lager heat input. Besides, the back gouging was a must for M process, which reduced the welding efficiency and the levels of standardization and automation of welding. By contrast, no groove preparation and back gouging were needed for H process.

The welding efficiency here was defined as the time required for welding the unit length (1 m) 30-mm-thick plate. It could be calculated for M process (η_m) and H process (η_h) as follows. Setting aside the time consumed in back gouging of M process, the efficiency of H process was still near four times higher than that of M process.

$$\eta_m = 6 \times \left(\frac{1}{0.5}\right) = 12.0 \text{ min/m} \tag{1}$$

$$\eta_h = 2 \times \left\{\left(\frac{1}{0.6}\right) + \left(\frac{1}{0.5}\right)\right\} = 3.7 \text{ min/m} \tag{2}$$

The heat input meant that the energy inputted to the unit length (1 m) weld of the 30-mm-thick plate. It could be calculated for M process (E_m) and H process

(E_h) as follows. The results showed that the heat input of H process was 18% less than that of M process.

$$E_m = 60 \times \{(244 \times 21.6 + \cdots + 313 \times 23.1)/0.5\}$$
$$= 4.49 \text{ kJ/mm} \tag{3}$$

$$E_h = 60 \times 2 \times \{(10000 + 1500)/0.6 + (266 \times 22)/0.5\} = 3.70 \text{ kJ/mm} \tag{4}$$

The weld areas were calculated by the software Image-Pro Plus. The weld area of H process was 34% smaller than that of M process. As everybody knew, the weld joint of Al 5083 alloy showed poor performances due to the softening effect. So the better performances could be expected for the weld joint with smaller weld area.

In brief, the hybrid laser-MIG welding plus MIG welding process developed in this research showed overwhelming superiorities over the MIG welding, which will be promising to be applied in industrial production.

4 Conclusions

In this study, the hybrid laser-MIG welding plus MIG welding process was established step by step. The maximum weld penetration, 18 mm, was obtained under the parameters of laser power 10 kW, welding speed 0.6 m/min and welding current 136 A. Based on which, double-sided hybrid laser-MIG welding method was designed and applied to the 30-mm-thick Al 5083 alloy butt joint. The investigation about groove types elucidated that the existence of gap or bevel had little effect on porosity, but exacerbated the weld undercut and even gave rise to the weld underfill. Then, the process was optimized by overlaying a MIG welding upon the weld. Analysis on the weld revealed that the overlaid MIG welding played multiple roles, including refining grains, eliminating the keyhole-induced porosities as well as making up the bead formations. Along the longitudinal direction of the weld, the

Table 2 Comparison between MIG welding and hybrid laser-MIG welding plus MIG welding

	MIG welding (M)	Hybrid laser-MIG welding plus MIG welding (H)
Groove preparation	Symmetric V-type (60°)	–
Back gouging	Need	–
Welding efficiency (min/m)	12.0	3.7
Heat input (kJ/mm)	4.49	3.70
Weld area (mm^2)	435	286

grains became finer from two fringes to the middle, and the microhardness, ductility, yield strength and tensile strength improved accordingly. The comparison between MIG welding process and hybrid laser-MIG welding plus MIG welding process indicated that the latter showed overwhelming superiorities over the traditional MIG welding, which will be promising in industrial applications.

Publisher's Note Springer Nature remains neutral with regard to jurisdictional claims in published maps and institutional affiliations.

References

1. Huang L, Wu D, Hua X, Liu S, Jiang Z, Li F, Wang H, Shi S (2018) Effect of the welding direction on the microstructural characterization in fiber laser-GMAW hybrid welding of 5083 aluminum alloy. J Manuf Process 31:514–522

2. Huang L, Hua X, Wu D, Jiang Z, Li F, Wang H, Shi S (2017) Microstructural characterization of 5083 aluminum alloy thick plates welded with GMAW and twin wire GMAW processes. Int J Adv Manuf Technol 93(5–8):1–9

3. Kim C, Ahn Y, Lee KB, Kim D (2016) High-deposition-rate position welding of Al 5083 alloy for spherical-type liquefied natural gas tank. Proc Inst Mech Eng B: J Eng Manuf 230(5):818–824

4. Zhiyong L, Srivatsan TS, Yan LI, Wenzhao Z (2013) Coupling of laser with plasma arc to facilitate hybrid welding of metallic materials: a review. J Mater Eng Perform 22:384–395

5. Gao Z, Wu Y, Huang J (2009) Analysis of weld pool dynamic during stationary laser–MIG hybrid welding. Int J Adv Manuf Technol 44(9–10):870–879

6. Wang X, Li B, Li M, Huang C, Chen H (2017) Study of local-zone microstructure, strength and fracture toughness of hybrid laser-metal-inert-gas-welded A7N01 aluminum alloy joint. Mater Sci Eng A 688:114–122

7. Zhang C, Gao M, Jiang M, Zeng X (2016) Effect of weld characteristic on mechanical strength of laser-arc hybrid-welded Al-Mg-Si-Mn aluminum alloy. Metall Mater Trans A 47:5438–5449

8. Ola O, Doern F (2015) Keyhole-induced porosity in laser-arc hybrid welded aluminum. Int J Adv Manuf Technol 80:3–10

9. Norris JT, Robino CV, Hirschfeld DA, Perricone MJ (2011) Effects of laser parameters on porosity formation: investigating millimeter scale continuous wave Nd:YAG laser welds. Weld J 90:198–203

10. Berger P, Hügel H, Graf T (2011) Understanding pore formation in laser beam welding. Phys Procedia 12:241–247

11. Bunaziv I, Akselsen OM, Salminen A, Unt A (2016) Fiber laser-MIG hybrid welding of 5 mm 5083 aluminum alloy. J Mater Process Technol 233:107–114

12. Leo P, Renna G, Casalino G, Olabi AG (2015) Effect of power distribution on the weld quality during hybrid laser welding of an Al–Mg alloy. Opt Laser Technol 73:118–126

13. Wu D, Hua X, Li F, Huang L (2017) Understanding of spatter formation in fiber laser welding of 5083 aluminum alloy. Int J Heat Mass Transf 113:730–740

14. Blecher J, Palmer T, DebRoy T (2015) Mitigation of root defect in laser and hybrid laser-arc welding. Weld J 94(3):73–82

15. Bachmann M, Avilov V, Gumenyuk A, Rethmeier M (2014) Experimental and numerical investigation of an electromagnetic weld pool support system for high power laser beam welding of austenitic stainless steel. J Mater Process Technol 214:578–591

16. Shiganov IN, Misyurov AI, Trushnikov AN, Kholopov AA, Blinkov VV (2017) Hybrid laser-arc welding of aluminium alloys. Weld Int 31:67–70

17. Wahba M, Mizutani M, Katayama S (2016) Single pass hybrid laser-arc welding of 25mm thick square groove butt joints. Mater Des 97:1–6

18. Faraji AH, Goodarzi M, Seyedein SH, Maletta C (2016) Effects of welding parameters on weld pool characteristics and shape in hybrid laser-TIG welding of AA6082 aluminum alloy: numerical and experimental studies. Weld World 60:137–151

19. Zhang C, Gao M, Wang D, Yin J, Zeng X (2017) Relationship between pool characteristic and weld porosity in laser arc hybrid welding of AA6082 aluminum alloy. J Mater Process Technol 240:217–222

20. Lakshminarayanan AK, Balasubramanian V, Elangovan K (2009) Effect of welding processes on tensile properties of AA6061aluminium alloy joints. Int J Adv Manuf Technol 40(3):286–296

21. Dutra JC, e Silva RH, Savi BM, Marques C, Alarcon OE (2015) Metallurgical characterization of the 5083H116 aluminum alloy welded with the cold metal transfer process and two different wire-electrodes (5183 and 5087). Weld World 59:797–807

22. Jiang Z, Hua X, Huang L, Wu D, Li F (2017) Effect of multiple thermal cycles on metallurgical and mechanical properties during multi-pass gas metal arc welding of Al 5083 alloy. Int J Adv Manuf Technol 93(1–13):3799–3811